ELSEVIER

Biophysical Chemistry 132 (2008) 69–80

Biophysical Chemistry

http://www.elsevier.com/locate/biophyschem

Study on the molecular mechanism of inhibiting HIV-1 integrase by EBR28 peptide via molecular modeling approach

Jian Ping Hu [a,b], Xin Qi Gong [a], Ji Guo Su [a,c], Wei Zu Chen [a], Cun Xin Wang [a,*]

[a] College of Life Science and Bioengineering, Beijing University of Technology, Beijing 100022, China
[b] Department of Chemistry and Life Science, Leshan Normal University, Leshan 614004, China
[c] College of Science, Yanshan University, Qinhuangdao 066004, China

Received 24 August 2007; received in revised form 21 September 2007; accepted 21 September 2007
Available online 29 September 2007

Abstract

Human immunodeficiency virus type 1 (HIV-1) integrase (IN) is an essential enzyme in the HIV-1 lifecycle which aids the integration of viral DNA into the host chromosome. Recently synthesized 12-mer peptide EBR28, which can strongly bind to IN, is one of the most potential small peptide leading compounds inhibiting IN binding with viral DNA. However, the binding mode between EBR28 peptide with HIV-1 IN and the inhibition mechanism remain uncertain. In this paper, the binding modes of EBR28 with HIV-1 IN monomer core domain (IN_1) and dimmer core domain (IN_2) were investigated by using molecular docking and molecular dynamics (MD) simulation methods. The results indicated that EBR28 bound to the interfaces of the IN_1 and IN_2 systems mainly through the hydrophobic interactions with the β3, α1 and α5 regions of the proteins. The binding free energies for IN_1 with a series of EBR28 mutated peptides were calculated with the MM/GBSA model, and the correlation between the calculated and experimental binding free energies is very good (r=0.88). Thus, the validity of the binding mode of IN_1 with EBR28 was confirmed. Based on the binding modes, the inhibition mechanism of EBR28 was explored by analyzing the essential dynamics (ED), energy decomposition and the mobility of EBR28 in the two docked complexes. The proposed inhibition mechanism is represented that EBR28 binds to the interface of IN_1 to form the IN_1_EBR28 complex and preventes the formation of IN dimmer, finally leads to the partial loss of binding potency for IN with viral DNA. All of the above simulation results agree well with experimental data, which provide us with some helpful information for designing anti-HIV small peptide drugs.

Keywords: Integrase; EBR28 peptide; Inhibition mechanism; MM/GBSA model; Molecular dynamics simulation; Essential dynamics

1. Introduction

Human immunodeficiency virus type 1 (HIV-1) is the etiological agent of AIDS [1,2]. The current antiviral strategy, i.e., cocktail treatment method, involves the combination of drugs that can inhibit the reverse transcriptase (RT) and the protease (PR). This strategy can decrease the viral blood concentration and the death rate of the AIDS patient as well. However, it can not completely deracinate the virus. Especially, the emergences of both drug resistance and viral high mutation make it necessary to identify additional targets and develop new classes of antiviral compounds. HIV-1 Integrase (IN) is such an attractive and important target, and is an essential enzyme in the HIV-1 lifecycle responsible for inserting the reverse-transcribed viral genome into the host DNA [3]. Unlike PR and RT, there is neither known functional analog of IN in human cells nor apparent cellular toxicity for IN inhibitor. Furthermore, IN adopts a single active site to fit two different DNA substrates (i.e., viral DNA and host DNA), which decreases the probability of drug resistance to its inhibitor to some extent [4].

HIV-1 IN encoded by the *pol* gene is composed of 288 residues and its molecular weight is 32-KDa. IN folds into three distinct functional domains: the N-terminal domain (residues 1–49), the catalytic core domain (residues 50–212), and the C-terminal domain (residues 213–288). So far, the structures of IN three distinct parts were solved through X-ray and NMR spectroscopy methods [5–7]. IN catalyzes the integration reaction in two steps. The first step is termed as 3′ end processing [8], in which two

* Corresponding author. Tel.: +86 10 67392724; fax: +86 10 67392837.
E-mail address: cxwang@bjut.edu.cn (C.X. Wang).

0301-4622/$ - see front matter © 2007 Published by Elsevier B.V.
doi:10.1016/j.bpc.2007.09.008

nucleotides are first removed from each 3′-end of each strand of viral DNA to produce new hydroxyl ends (CA-3′OH). The second step named DNA strand transfer occurs in the nucleus [9], where the recessed 3′-ends of viral DNA are covalently joined to the host DNA. Chen et al. successfully resolved the fragment structure of the IN dimmer comprising the C-terminal domain and the catalytic core domain and found that the strip of positive potential continued through residues K173, K159, K186 and K188 out to the residues K211, K219, K243 and K263 of the paired monomer. It was proposed that the minimal IN structure for binding with viral DNA is dimmer [10,11].

In view of the successful application of peptide drug to treat AIDS, the study on peptide inhibitors of HIV-1 IN is one of the focuses of the international scientific research fields. Soultrait et al. successfully selected a short peptide of 33 residues (I33), which can tightly bind to IN, through the yeast two-hybrid system experiment [12]. The inhibitory potency of I33 peptide is improved with a 12-mer peptide (EBR28) corresponding to its amino terminal part. Alanine substitution of each amino acid of EBR28 indicated that hydrophobic residues were important for the inhibition. EBR28 can prevent HIV-1 IN from interacting with viral DNA through binding to the core domain of the enzyme and the IC50 value is 5 μM. It is generally believed that EBR28 is one of the most potential peptide leading compounds of anti-IN inhibitor [13].

The previous studies have only proposed the conclusion that EBR28 can inhibit HIV-1 IN from binding to viral DNA by interacting with the core domain of IN, however, not given the clear inhibition mechanism [12]. In this work, the structure of EBR28 was constructed from the NMR experimental data [12], then the binding modes between the peptide with the core domain of IN monomer (IN_1) and that of IN dimmer (IN_2) were predicted by using RosettaDock method [14]. The structures of the two docked complexes (i.e., IN_1_EBR28 and IN_2_EBR28) were refined via molecular dynamics (MD) simulation approach. The binding free energies for IN_1 with a series of EBR28 mutated peptides were calculated with the MM/GBSA model in order to confirm the binding mode of IN_1 with EBR28. By comparatively analyzing the four MD trajectories (i.e., IN_1, IN_2, IN_1_EBR28 and IN_2_EBR28), the definite molecular inhibition mechanism of EBR28 to HIV-1 IN was proposed, and this mechanism was consistent with all the experimental data obtained up to now. Fig. 1 shows the procedure of our work.

2. Methods

2.1. Docking

Two docking studies were performed for EBR28 with IN_1 and IN_2 with RosettaDock 1.0 package [14]. Each docking was

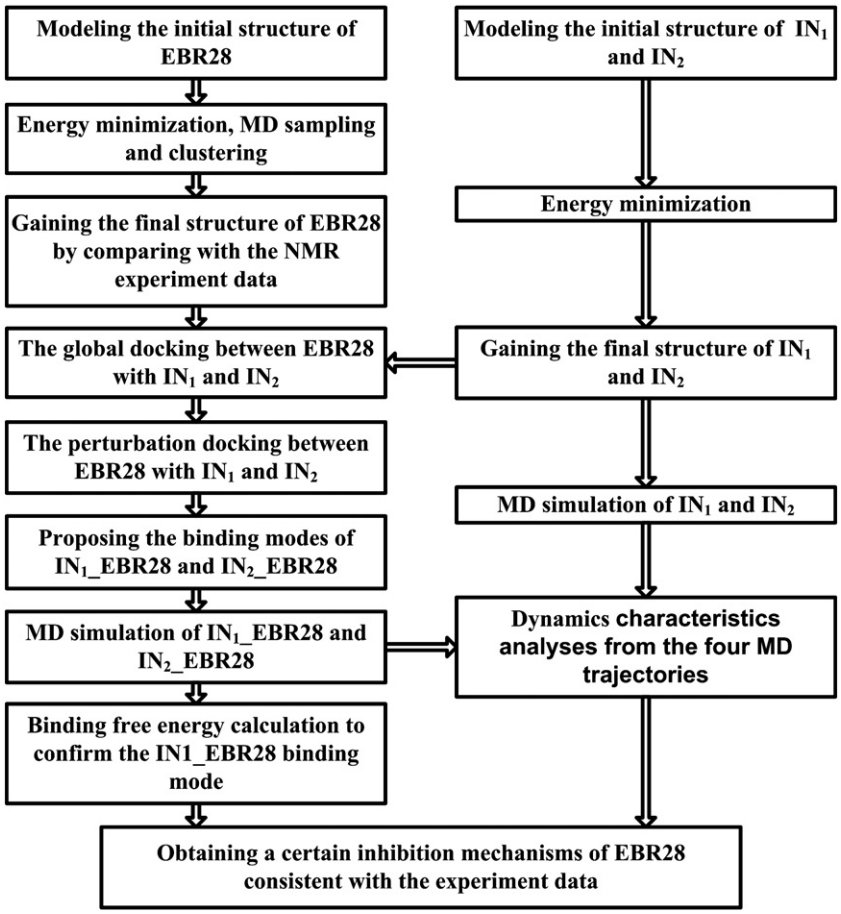

Fig. 1. Protocol for the prediction of the molecular mechanism of inhibiting HIV-1 IN induced by EBR28 peptide.

set to two stages, i.e., the global docking and perturbation docking. In the global docking, RosettaDock first employed a low resolution rigid body Monte Carlo (MC) search. Then, it was followed by an all atom simultaneous optimization of backbone displacement using a rigid body Monte Carlo Minimization and the side chain rotamer conformations with a packing algorithm [15]. 10^5 independent MC searches were carried out and the decoy selected as the initial structure for the following perturbation docking was obtained by considering its energy scoring and clustering comprehensively. The perturbation docking study repeated 2×10^3 times was performed to select the final docking complex and its parameters were set as default values [14].

So far, the performance of the RosettaDock algorithm has been successfully tested in several rounds of CAPRI [16,17]. If a protein exhibits comparatively low flexibility and there is some helpful biological information, the result of protein–protein docking is more credible [18].

2.2. Ligand setup

The structure of EBR28 peptide was generated with Jackal program [19]. After 5000 steps of the steepest descent followed 5000 steps of the conjugate gradients energy minimizations, one 1100 ps MD simulation (including 100 ps restraint MD simulation) was performed. Snapshots were extracted from the trajectory every 0.5 ps from 100 to 1100 ps. The snapshots within a 0.1 nm clustering threshold were designated as a set. The structure with the lowest potential energy in the maximum cluster was used for the following molecular docking. Analyzed through the DSSP package [20], the predominant secondary structure of residues 1–10 in EBR28 was an α-helix while that of residues 11–12 was a random coil. It was also found that all the hydrophobic residues were located on one side of the α-helix and the more hydrophilic ones on the other side (Fig. 2). In a word, the modeled structure of EBR28 was consistent with the optimal structure obtained from NMR experiment [12]. Also, a series of EBR28 mutated peptides were obtained from the same protocols mentioned above.

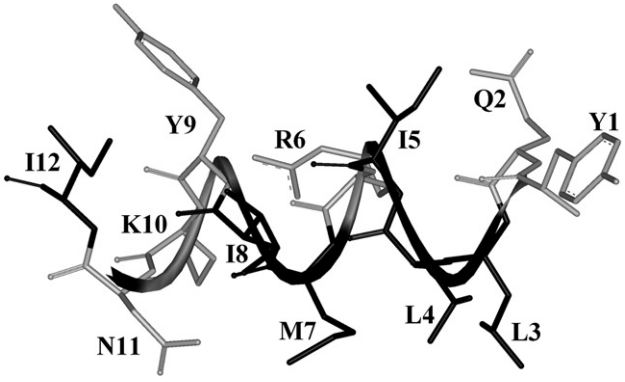

Fig. 2. The initial structure of EBR28 for molecular docking. EBR28 is displayed with the solid-ribbon model, the stick model and one-letter representation are used to describe the residues. The hydrophobic residues are shown in black and the hydrophilic ones in gray.

AGADIR is a prediction algorithm based on the helix/coil transition theory [21]. AGADIR can be used to predict the helical behavior of monomeric peptides only through considering short range interactions. In this work, the helical content of EBR28 was explored with this method. Fig. 3 shows the relative tendency of forming helix in each residue of EBR28. It is found that the helix property of residues 1–8 in EBR28 is higher than that of residues 9–12, which also confirm the validity of the modelled ligand structure by and large.

2.3. Protein setup

The structure of the IN_2 system was built from the X-ray crystal tetramer structure (PDB code: 1 K6Y) [7]. The core domains of chain A and B were kept and the unresolved residues 50–55 and 140–148 were modeled from the homologous structure of chain A of the crystal structure 1WJD [22] and chain B of 1BIS [23]. The position of the first Mg^{2+}ion was consistent with that of Zn^{2+}ion in 1 K6Y, while the second Mg^{2+}ion was placed in the same relative position according to the high homologous PDB structure of 1VSH [24]. Thus, the IN_2 system containing two Mg^{2+}ions was obtained. Then, the structure was minimized by 5000 steps of the steepest descent and the conjugate gradient energy minimization, respectively. After removing chain B of IN_2, we employed the same energy minimization strategy to the rest (i.e., IN_1) once again. Thus, the structures of both IN_1 and IN_2 were obtained as the initial receptors for the following molecular docking.

2.4. Molecular dynamics simulations

Four independent MD simulations were carried out for the IN_1, IN_2, IN_1_EBR28 and IN_2_EBR28 systems using the AMBER 8 suite of programs [25,26] with the AMBER force field [25, 27–30]. In each simulation, the solute was solvated in a truncated periodic box with a 0.8 nm solute-wall distance using the TIP3P water model [31]. Before MD simulations, two stages of minimization were performed for the initial structures. First, the solute atoms were restrained by the force constant 2.09×10^5 kJ·mol^{-1}·nm^{-2}. Water molecules were minimized for 250 steps with the steepest descent method followed by 750 steps of the conjugate gradient. Then, the restraint for the solute was removed and 2500 steps energy minimization of the steepest descent followed by 2500 steps of the conjugate gradient were carried out for the total system. The convergence criterion was 4.182 kJ·mol^{-1}·nm^{-1}.

MD simulations were set to two stages. First, we restrained the solutes (the restraining force constant was 4.18×10^3 kJ·mol^{-1}·nm^{-2}) and slowly heated the systems up from 0 K to 300 K over 100 ps. Then, non-restraint MD simulations at 300 K were performed for 1900 ps. In these simulations, the system structures were monitored simultaneously with the SYBYL software. The SHAKE algorithm [32] was applied to constrain all bonds and a 1.2 nm cutoff was used for all non-bonded interactions. The MD time step was taken as 2 fs.

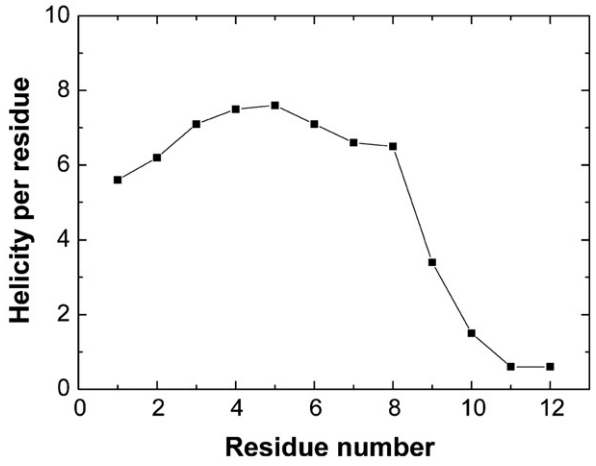

Fig. 3. The helicity per residue for EBR28 by the program of AGADIR.

2.5. Essential dynamics

The complexity of molecular motions observed in MD simulations can be simplified by essential dynamics (ED) analyses [33–36], which separates the configurational space into two subspaces. The first subspace is the essential subspace where large amplitude global anharmonic motions comprising most of the positional fluctuations occur. In the unessential one, there are high-frequency local motions which have a narrow Gaussian distribution. The local motions are restrained and harmonic in nature, and they contain less functional information.

In this work, ED analyses were performed for the Cα atoms in the IN_1, IN_1–EBR28, IN_2 and IN_2–EBR28 systems based on the MD trajectories from 100 to 2000 ps. After eliminating the overall translation and rotation, four covariance matrixes were constructed and their sizes were $489\times489\times489$, $525\times525\times525$, $978\times978\times978$ and $1014\times1014\times1014$, respectively. Then, the diagonalization of the four matrixes led to 163, 175, 326 and 338 eigenvalues, and their corresponding eigenvectors as well. In the end, the projection of the displacements on each eigenvector showed the width of the essential space explored by the system as a function of time [33–36].

2.6. MM/GBSA methodology and energy decomposition

The MM/GBSA method [37, 38] was used to calculate the binding free energy between IN and its substrate EBR28 peptide. 50 snapshots were extracted from the trajectory every 50 ps from 1050 to 2000 ps in order to calculate the mean binding free energy. The formula was used as:

$$\Delta G_{\text{bind}} = \Delta E_{\text{MM}} + \Delta\Delta G_{\text{sol}} - T\Delta S$$

where ΔG_{bind} is the binding free energy, and ΔE_{MM} denoted the sum of molecular mechanical energies in vacuo and could be further divided into the contributions from electrostatic, van dew Waals, and internal energies. This term could be computed through molecular mechanics method. $\Delta\Delta G_{\text{sol}}$ is the solvation free energy which includes the polar solvation free energy calculated with the Generalized Born (GB) approximation model [39–41] and the non-polar part obtained by fitting solvent accessible surface area (SASA) [42]. The last term in the above equation, i.e., $T\Delta S$ is the solute entropy which is usually estimated by normal mode analysis method [43].

The essential idea of energy decomposition was to decompose the energy contribution of each residue from the association of the receptor with the ligand into three parts. The molecular internal energy in vacuo was computed with the molecular mechanics method. The polar contribution of solvation free energy was calculated with the Generalized Born (GB) approximation model [39–41]. The nonpolar solvation part was obtained with the LCPO model [44,45]. Additionally, all the energies were decomposed into backbone and side-chain atoms. Through energy decomposition, we can analyze the contributions of the key residues to the binding.

3. Results and discussion

3.1. Binding modes prediction

By observing the top 200 lowest energy structures selected from the 10^5 decoys provided by global docking, it is found that all ligands located in the middle of the interface of the IN_1 and IN_2 systems. The final docking results have the lowest score in the most highly populated cluster, and the RMSD tolerance for the cluster analysis is 0.3 nm.

Fig. 4 shows the binding modes between EBR28 with IN_1 and IN_2, which excludes the probable binding modes proposed by Soultrait et al. [12]. As suggested by by Soultrait, EBR28 may competitively bind to the same catalytic pocket, which is characterized by the conserved DD-35-E motif, in the core domain as is occupied by viral DNA. In our global dockings, none of this type of complex is observed. As shown from Fig. 4, the hydrophobic side of EBR28 faces the interface of IN_1, which is consistent with experimental data [12]. As for the IN_2–EBR28 system, the hydrophilic one locates near that of chain A of the IN_2 system (IN_a) while the hydrophobic side is up against the interface of chain B of the IN_2 system (IN_b).

Table 1 lists the contact residues of the IN_1–EBR28 and IN_2–EBR28 systems in the neighborhood of 0.4 nm of EBR28. As shown from Table 1, the contact residues mainly lie in the β3, α1 and α5 regions. The binding site of IN_1 with EBR28 is somewhat different from that of IN_2. Specially, the former is closer to α5 region (residues 172–184) and the latter slants from the β3 region (residue 83–89) and α1 region (residues 94–105) of IN_a to the α1 region of IN_b. It is unexpected that EBR28 can bind to IN_2 more deeply than to IN_1 since the steric hindrance of Y1 in EBR28 is obvious. Y1 seems to have the locating function by interacting with Q177 in the two complexes, which is also observed in the hydrogen bond analysis (see below).

3.2. Molecular dynamics simulation

Fig. 5 shows the potential energies and RMSD evolutions for the four MD simulation systems (IN_1, IN_1–EBR28, IN_2 and IN_2–EBR28). The potential energies of the four systems are stable after 200 ps. The mean values of the potential energies for the IN_1,

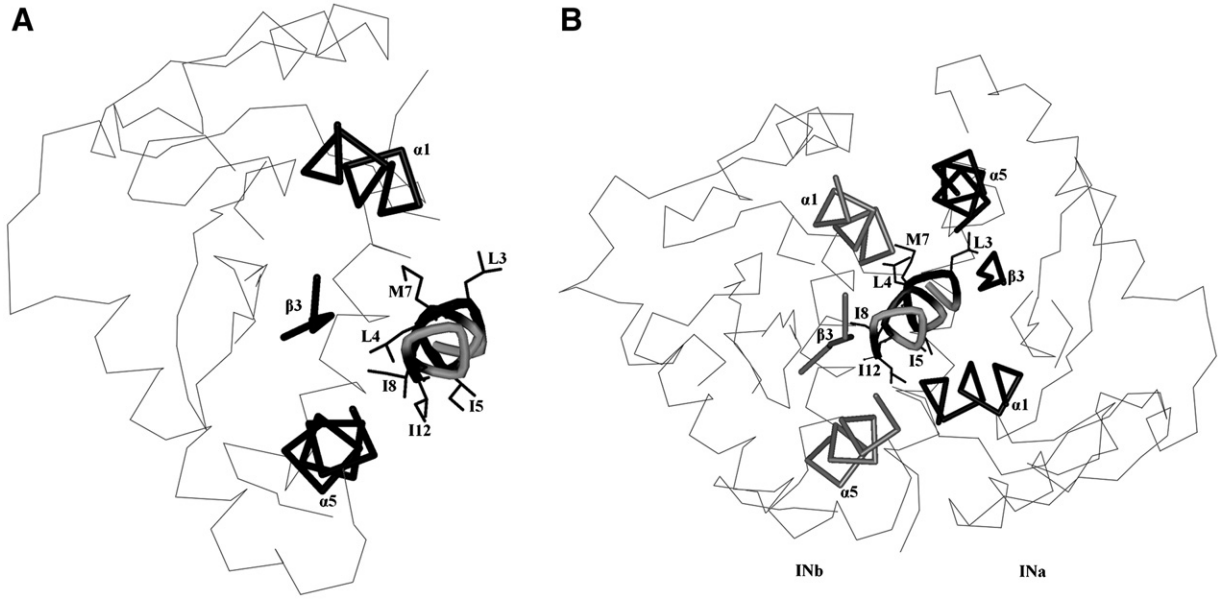

Fig. 4. The binding modes of EBR28 with (A) IN_1 and (B) IN_2. The structures of IN_1 and IN_2 are represented by a schematic model. EBR28 is displayed with solid-ribbon model.

IN_1–EBR28, IN_2 and IN_2–EBR28 systems are -2.648×10^5, -2.5×10^5, -3.686×10^5 and -3.67×10^5 kJ·mol^{-1}, respectively. Their corresponding standard deviations are 507, 489, 588 and 615 kJ·mol^{-1}, which account for the total values less than 0.2%. As shown from Fig. 5 (B), the RMSD values of Cα atoms in the IN_1, IN_1–EBR28, IN_2 and IN_2–EBR28 systems, which have been calculated after fitting the Cα atoms to the initial minimized structures, converge around 0.22, 0.23, 0.21 and 0.25 nm after 1500 ps. The RMSD values of the docked complexes, especially IN_2–EBR28, exhibit higher fluctuation. This may be caused by the high mobility of EBR28 (see the following motive difference analysis of EBR28).

3.3. The motive difference of EBR28 in the two binding modes

To explore the motility of EBR28, the RMSD values of Cα atoms in EBR28 have been calculated in the IN_1–EBR28 and IN_2–EBR28 systems. The mobility of EBR28 in IN_1–EBR28 is relatively weaker than that in IN_2–EBR28. In IN_1–EBR28, the RMSD values maintain around 0.075 nm from 100 to 1000 ps and reach about 0.1 nm at 1050 ps. In IN_2–EBR28, the mobility of EBR28 is relative higher, and the RMSD values fluctuate around 0.075 nm in the period of 100 to 1400 ps and there is an abrupt transition to 0.2 nm after 1400 ps. Thus, we superimpose the average structure of IN_1–EBR28 from 200 to 1000 ps onto that from 1100 to 2000 ps, and the average structure of IN_2–EBR28 from 200 to 1400 ps onto that from 1500 to 2000 ps. It can be seen in Fig. 6 that the positions of the catalytic pockets comprised of DD-35-E motif in the two docked complexes keep somewhat stable, while the conformation of EBR28 in the IN_2–EBR28 system undergoes more significant change than that of EBR28 in the IN_1–EBR28 system. Specifically, EBR28 exhibits visible rotation along Y1 and unobvious translation to outside.

In order to obtain the EBR28 movement characters in the IN_2–EBR28 systems further, the motion tendency angle (IN_a–EBR28–IN_b) is defined by the mass center of IN_a, the mass center of IN_b and the pivot formed by the mass center of EBR28. The subunit distances (IN_a–IN_b) are formed between the mass center of IN_a and that of IN_b in the IN_2–EBR28 and IN_2 systems. Fig. 7 shows the IN_a–IN_b distances and the IN_a–EBR28–IN_b angle as a function of simulation time. As for the IN_2 system, the IN_a–IN_b distance value is relative stable and the mean value is 2.06 nm. However, the distance in IN_2–EBR28 system exhibits a somewhat fluctuation around 2.11 nm. Thus, the subunit distance increase by about 0.05 nm after the association of EBR28. From Fig. 7 (B), it is also found that the IN_a–EBR28–IN_b angle gradually decreases from 58 to 54 degree.

In summary, the associations of EBR28 with both IN_2 and IN_1 have unobvious influence on the catalytic region. EBR28 is

Table 1
The interactions between each residue of EBR28 and the contact residues in the two docked complexes

EBR28	Contact residues of IN_2–EBR28	Contact residues of IN_1–EBR28
Y1	IN_a: E87, V88, K103	R107, Q177, F181, F185
	IN_b: E87, V88, Y99, K103, Q177	
Q2	IN_a: E87, V88, I89, P90, E96, F100	–
L3	IN_a: V88, P90	R107
L4	IN_b: E87, P90, E96	E85, A86, V180
I5	IN_a: Y99	–
	IN_b: K173	
R6	IN_a: P90	–
M7	IN_b: P90	K103
I8	IN_b: V88, I89, P90	K173, Q177
Y9	IN_b: Y99, H171	–
K10	–	–
N11	IN_b: P90	E87, V88, K173
I12	IN_b: H171	K173

[a]The sign of "–" indicates there is no contact residues for the systems.

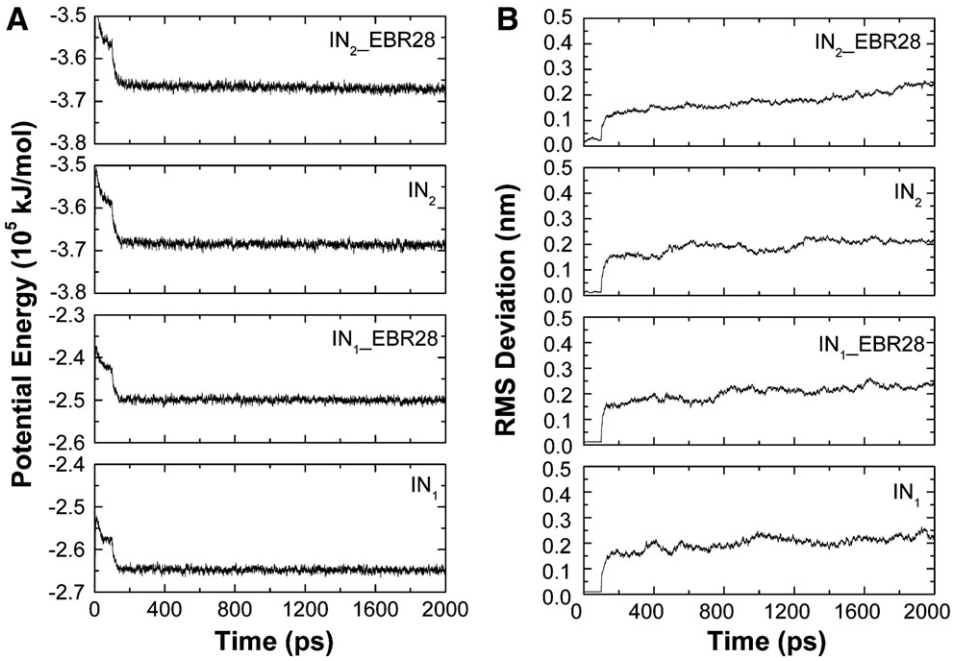

Fig. 5. MD simulations of the four systems in explicit water at 300 K. (A) Time evolution of the potential energies. (B) RMS Deviations comparing with the initial minimized structures as a function of time.

still stable after binding to the interface of IN_1. When EBR28 binds to IN_2, the subunit distance of IN_2 increases inconspicuously. In addition, EBR28 has a bit tendency of keeping away from IN_2 along with simulation.

3.4. Hydrogen bonding analysis

The subunit distance of IN_2 increases by about 0.05 nm after the association of EBR28. The hydrogen bonds between the two subunits in the IN_2 and IN_2_EBR28 systems were comparatively analyzed to explore the influence of the subunit distance change on the interactions between the two subunits. Herein, the geometric criteria [46] for the formation of hydrogen bonds are the angle of donor–hydrogen–receptor larger than 135° and the distance of donor–receptor less than 0.35 nm.

Table 2 lists all hydrogen bonds with the frequencies of occupancy over 50% between the two subunits in the IN_2 and the IN_2_EBR28 systems. As shown in Table 2, there are four hydrogen bonds whose occupancy frequencies are over 50% in the IN_2 system. As to the IN_2_EBR28 system, the corresponding

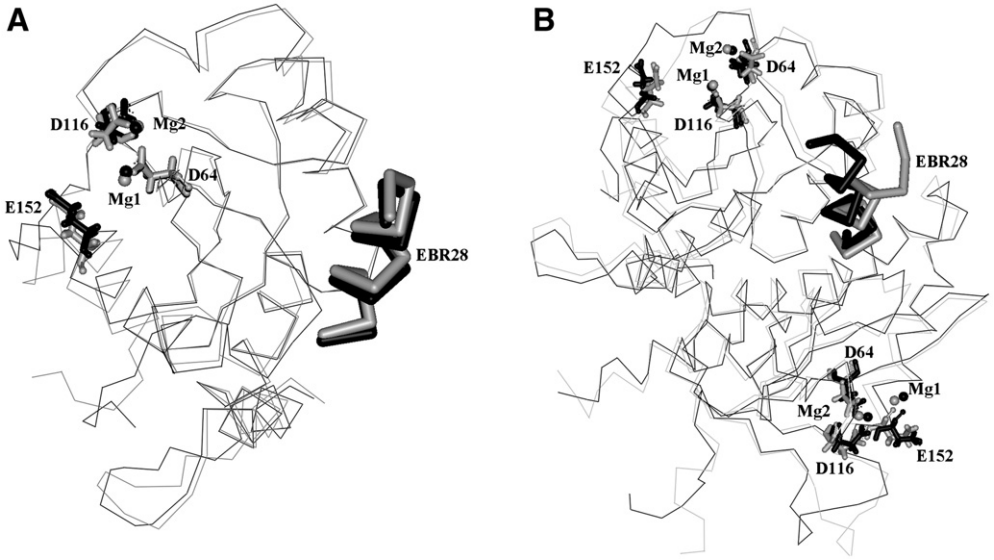

Fig. 6. The motive difference of EBR28 in the two binding modes. (A) Superimposition of the average structure in IN_1_EBR28 from 200 to 1000 ps (black line) upon that from 1100 to 2000 ps (gray line). (B) Superimposition of the average structure in IN_2_EBR28 from 200 to 1400 ps (black line) upon that from 1500 to 2000 ps (gray line). The stick model indicates the inhibitor EBR28, and the one-letter ball-stick model is used to represent the DD-35-E motif residues. Mg^{2+} ion is described with the CPK model.

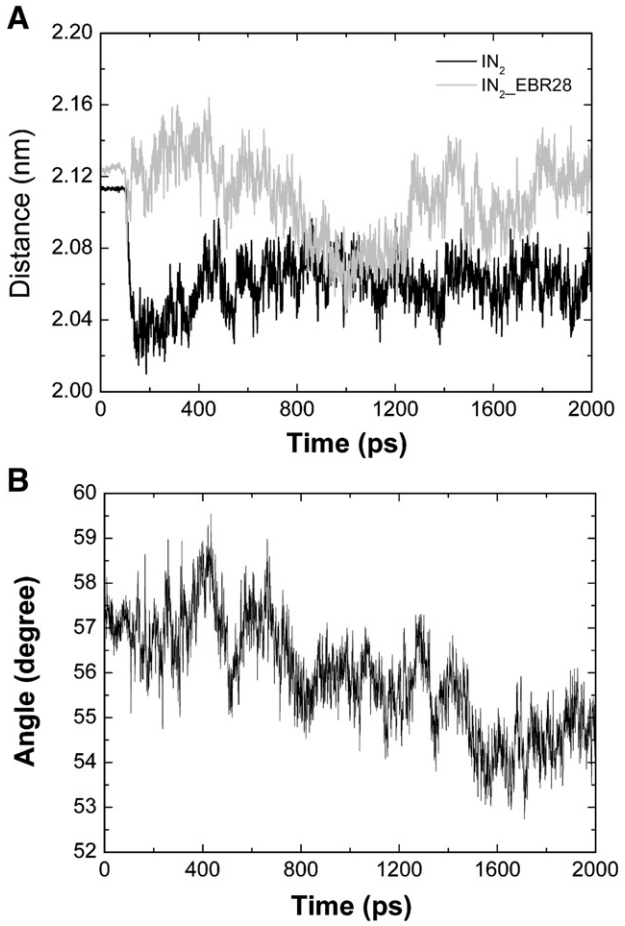

Fig. 7. The analysis of the subunit distances and the motion tendency angle. (A) The subunit distances as a function of time in the IN_2 and the IN_2_EBR28 systems. (B) The motion tendency angle as a function of time in the IN_2_EBR28 system.

amount of the hydrogen bonds is five. Thus, the number of hydrogen bonds between subunits does not decrease with the subunits remoteness from each other. Specifically, the hydrogen bonds between G106 with N184 and between Q168 with W132 maintain in the two systems. It is also found that the maximum contribution to the formation of hydrogen bonds is from the α1 and α5 regions of the proteins.

Comparing the hydrogen bonds involved in EBR28 of the IN_1_EBR28 and IN_2_EBR28 systems, it can be seen that the hydrogen bond between Y1 of EBR28 with Q177 exists in the two systems. Its occupancy frequency in the IN_1_EBR28 system is 88.09%, and that in the IN_2_EBR28 system is only 30.07%. The occupancy frequency of the hydrogen bonds between Y1 of EBR28 and V88 is also observed in the IN2_EBR28 system and its occupancy frequency is 86.71%. All the results are consistent with the above results obtained through contact residues analysis, which further shows the orientation potency of Y1.

3.5. Essential dynamics

To explore how the binding of EBR28 bear on the motions of IN_1 and IN_2, the four MD simulation trajectories from 100 to 2000 ps were used to perform ED analysis. After analyzing the top 20 eigenvalues as a function of its corresponding eigenvector index in the the IN_1, IN_1_EBR28, IN_2, IN_2_EBR28 systems. It is found that the eigenvalue distribution of IN_1 is very similar with that of IN_1_EBR28 and those of IN_2 and IN_2_EBR28 are similar also. Analyzing all eigenvalues indicates that over 65% of all motions are accounted for by the first four eigenvectors and 58% by the first three eigenvectors. Thus, the first three or four top motion models owning the top 3 or 4 large eigenvalue can be used to substitute the total motion through the motional contribution analysis. Then, four MD simulation trajectories were projected on each of the first four eigenvectors. The results show that the range of conformational space explored along each eigenvector is very similar for IN_1 and IN_1_EBR28, and those of IN_2 and IN_2_EBR28 are similar too. The narrow Gaussian displacement distribution which is the local harmonic motion character appears after the third eigenvectors, which indicates that the functional un-harmonic motions are correspond to the first three motions.

Fig. 8 shows the Cα displacement along the three main eigenvectors. It can be seen from Fig. 8 that the functional loop region (residues 139–149) and another loop region (residues 185–195) between the α5 region and α6 region exhibit relative high flexibility in the four systems. It is interesting that the interfaces of the IN_1_EBR28 and IN_2_EBR28 systems (i.e., β3

Table 2
The hydrogen bonds between the two subunits in the IN_2 and IN_2_EBR28 systems[a]

System	Acceptor[b]	Donor[c]	Dist.[d](nm)	Angle[e](°)	Freq.[f](%)
IN_2	G106-O	N184′-ND2-HD22	0.286±0.01	162.62±9.23	71.61
	R107-O	Y83′-OH-HH	0.281±0.01	170.79±9.19	70.27
	G106′-O	N184-ND2-HD22	0.287±0.01	171.82±9.29	62.45
	Q168′-OE1	W132-NE1-HE1	0.286±0.01	169.34±10.48	62.20
IN_2_EBR28	K173-O	Y99′-OH-HH	0.278±0.01	169.51±10.62	84.02
	G106-O	Y83′-OH-HH	0.279±0.01	164.81±8.51	72.73
	G106′-O	N184-ND2-HD22	0.287±0.01	161.14±9.11	64.74
	Q168′-OE1	W132-NE1-HE1	0.285±0.01	157.8±11.26	56.84
	Q177-OE1	R107′-NH2-HH22	0.278±0.01	154.3±12.69	52.85

[a] The hydrogen bonds pairs, whose frequencies of occupancy are over 50%, in the IN_2 and IN_2_EBR28 systems. single quotation mark is used to describe the residues of IN_b.
[b] Receptor atoms.
[c] Donor atoms.
[d] The donor–receptor distance.
[e] The angle of donor–hydrogen–receptor.
[f] The probability of hydrogen bond occurring in the MD simulation.

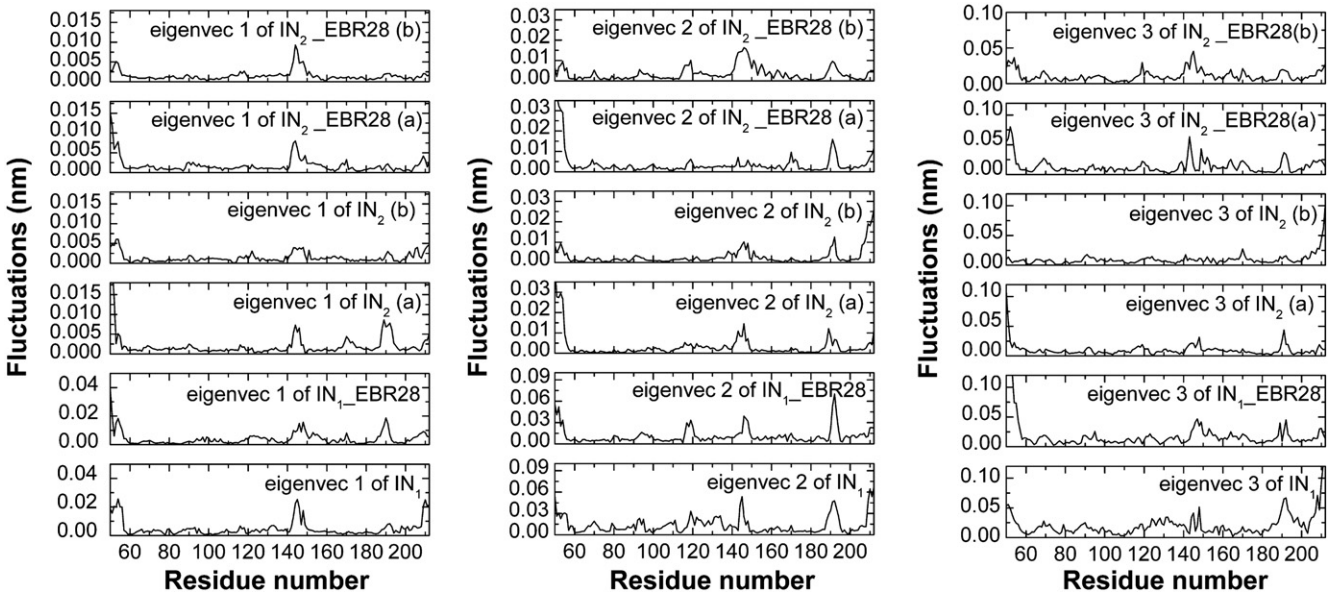

Fig. 8. Residue displacement caculated fore each Cα atom along the three main eigenvectors.

region, α1 region and α5 region) still display small flexibility in spite of the association with EBR28. The mobility of the conserved DD-35-E motif in the catalytic region is small and similar in the four systems.

It is noteworthy that the total motility of IN_2–EBR28 is somewhat higher than that of IN_2, which has correlation with the 0.05 nm separation between the two subunits of IN_2. Whereas as a whole, EBR28 binds to the low flexible region of the proteins (i.e., α1, α5 and β3 regions), therefore the motion models of IN_1 and IN_2 undergo unobvious change after the association with EBR28. These results exclude the assumption that the dysfunction of IN results from the change of motional modes [12].

3.6. Binding free energy calculation for IN_1 with a series of mutated peptides

The binding free energies between IN_1 and a series of EBR28 mutated peptide were calculated by using MM/GBSA method. It is noteworthy that the entropy values for IN_1–EBR28 is estimated by the normal-mode analysis method [43], while those of the other mutated complexes are fitted with the semi-empirical method proposed by Andrew [47].

Table 3 lists the exact contribution to binding free energy. By analyzing the non-polar interaction values ($\Delta E_{vdw}+\Delta G_{SA}$) and the polar interaction one ($\Delta E_{coul}+\Delta G_{GB}$), it is found that the associations between IN_1 and a series of peptides are mainly

Table 3
Binding free energy values for IN with a series of mutated peptides

Compd.[a]	ΔE_{vdw}[b]	ΔE_{coul}[c]	ΔG_{SA}[d]	ΔG_{GB}[e]	$-T\Delta S$[f]	ΔG_{cal}	ΔG_{exp}	$\Delta\Delta G$[g]
IN_1–EBR28	−249.3	−369.2	−35.6	462.1	157.5	−34.5	−30.6	−3.9
IN_1–Q2A	−241.7	−390.4	−36.5	487.5	150.3	−30.8	−29.3	1.5
IN_1–L3A	−237.7	−275.6	−35.5	379.7	154.6	−14.5	−21.6	7.1
IN_1–L4A	−248.5	−378.3	−35.6	476.6	154.6	−31.2	−27.9	−3.3
IN_1–I5A	−232.4	−453.8	−36.4	559.2	154.4	−9.01	−24.9	13.9
IN_1–R6A	−231.8	−589.7	−35.3	680.0	149.7	−27.1	−25.7	−1.4
IN_1–M7A	−216.2	−476.3	−34.2	551.9	151.4	−23.4	−23.9	0.5
IN_1–I8A	−249.3	−416.2	−36.5	519.4	154.4	−28.2	−25.6	−2.6
IN_1–Y9A	−236.5	−360.6	−35.1	461.0	152.8	−18.4	−25.3	6.9
IN_1–K10A	−225.3	−803.5	−33.9	875.8	149.6	−37.3	−28.5	−8.8
IN_1–N11A	−253.6	−336.2	−35.7	430.8	153.2	−41.5	−29.6	−11.9
Mean	−238.4	−440.9	−35.5	534.9	152.9	−26.9	−26.6	5.62

[a] The sequences of the native EBR28 and mutated peptides are the same as de Soultrait's work [12].
[b] van der Waals energy.
[c] Electrostatic energy.
[d] Hydrophobic contribution to solvation free energy.
[e] Hydrophilic contribution to solvation free energy.
[f] Conformational entropy multiplied by temperature.
[g] The difference between calculated binding free energy (ΔG_{cal}) and the corresponding experimental value (ΔG_{exp}). The unit of all the values is kJ/mol.

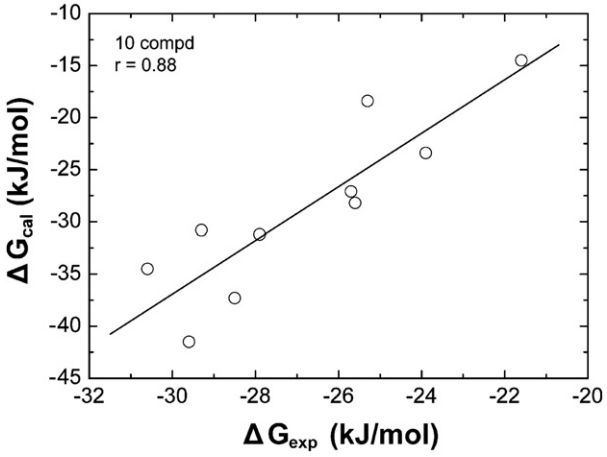

Fig. 9. Correlation between the calculated and experimental binding free energies for IN with a series of peptides.

driven by the favorable non-polar interaction while the polar interactions are unfavorable to ligand binding.

Fig. 9 shows a majority of the calculated ΔG_{cal} values have good correlations with the experimental values, except for the I5A and N11A systems whose errors are 13.9 and −11.9 kJ/mol, respectively. If the high error value of I5A is not taken into account, the average absolute error between predicted values and experimental values is 4.79 kJ/mol, and the coefficient of linear regression is 0.88. These results are similar with that reported by Kuhn and Hou [48,49]. In Kuhn's work with nine inhibitors of avidine and streptavidin, the predicted ΔG values have a good correction with its corresponding experimental one. The correlation between the calculated and experimental ΔG is 0.92, but the mean error reaches 15.9 kJ/mol. In Hou's work with eight hydroxamate inhibitor and MMP-2, the coefficient is 0.84 and the mean error is 8.9 kJ/mol.

Considering the good correlation of the calculated and experimental binding free energies, the docked IN_1–EBR28 complex structure is creditable. Presently, the docking between a protein and a small peptide is a challenging question, and the main difficulty lies in the high flexibility of small peptide [18] which makes it hard to determine its predominant conformation. In this work, EBR28 tends to form a stable α-helix (see Fig. 2). The initial EBR28 structure before docking obtained after MD sampling, is in agreement with that provided by NMR experiment [12]. The superimposing and ED analysis mentioned above show that the IN conformation doesn't undergo significant change in spite of the association with EBR28. If the receptor and ligand exhibit small flexibility, this type of unbound docking is relatively easy [18]. Thus, a good docked result can be obtained finally in this work.

3.7. The interactions between interfaces of the IN_1–EBR28, IN_2, IN_2–EBR28 systems

To explore the interfacial interactions and key residues to the association, the energy decomposition method is used to calculate the contribution of each residue to the formation of the three complexes (i.e., the IN_1–EBR28, IN_2 and IN_2–EBR28 systems). Herein, the binding energy includes the solvent effect.

Fig. 10A–B shows the contribution of each residue to the dimerization of IN. For simplified analysis, IN_a is regarded as the receptor and IN_b is treated as the ligand. As shown in Fig. 10A–B, the total binding energy is −441.2 kJ/mol. Specifically, the dimerization is primary dependent on the interactions involved by the β3 region (residues 84–89), α1 region (residues 94–105) and α5 regions (residues 172–185), which is similar with the result gained by hydrogen bond analysis and is also consistent with the experimental data [50].

Fig. 10C–D shows the contribution of each residue to the formation of the IN_1–EBR28 complex, in which IN_1 is taken for the receptor and EBR28 is regarded as the ligand. Summed from Fig. 10C–D, the total binding energy is −192.0 kJ/mol. The non-polar residues (i.e., L3, L4, M7, I8 and N11) are essential for the IN_1–EBR28 system stabilization. The binding energies of residues Y1, Q2 and K10 in EBR28 are positive, especially that of K10 reaches 6.6 kJ/mol, which further proves that the polar interactions are unfavorable for the formation of IN_1–EBR28. As for IN_1, the key residues are Q177, K173, F100, L104, E85 and Y83, whose binding energies are −17.0, −16.7, −4.02, −2.8, −20.4 and −8.1 kJ/mol, respectively. Obviously, all these key residues lie in the the β3, α1 and α5 regions. The residues which are most unfavorable for the association were K10 of EBR28 and K103 of IN_1, whose binding energies were 6.6 and 5.9 kJ/mol, respectively. By comparing the binding energy decomposition analyses of IN_2 and IN_1–EBR28, it is found that EBR28 in the IN_1–EBR28 system serves as the substitute for the other subunit of IN_2.

Two models are used to analyze the interactions between the interfaces of the IN_2–EBR28 system. In model 1, IN_2 is regarded as the receptor and EBR28 is taken for the ligand. In model 2, IN_a–EBR28 is as the receptor and IN_b is as the ligand. After the calculation, the binding energy is −59.0 kJ/mol in the model 1 and −516.6 kJ/mol in the model 2. By comparing the binding energy of the model 1 with that of IN_1–EBR28, it can be seen that the association of EBR28 with IN_2 is weaker than that with IN_1. From the comparison of the binding energy of model 2 with that of IN_2, the interactions between the two subunits in the IN_2 still keep stable in spite of the association with EBR28, which is consistent with the conclusion by the hydrogen bonds analysis. Though the association of EBR28 with IN_2 makes the two subunits separate 0.05 nm, the dissociation and subunit structure change of IN_2 are hardly observed.

Fig. 10E reports the contribution of each residue to the formation of the IN_2–EBR28 complex from the two models. Based on the model 1, the non-polar residues (I5 and I8) of EBR28 favor binding with IN_2. The α1 and β3 regions of IN_2 aid the association with EBR28 while the contribution of α5 region is very small, which may have correlation with the binding site of EBR28 in the vicinity of the β3 region. From the model 2, some non-polar residues (L4, I5 and I8) of EBR28 are the key residues which aid the association. It is also found that the α1, β3 and α5 regions of IN_b is more important than those of IN_a for the formation of IN_2–EBR28, which may be relative

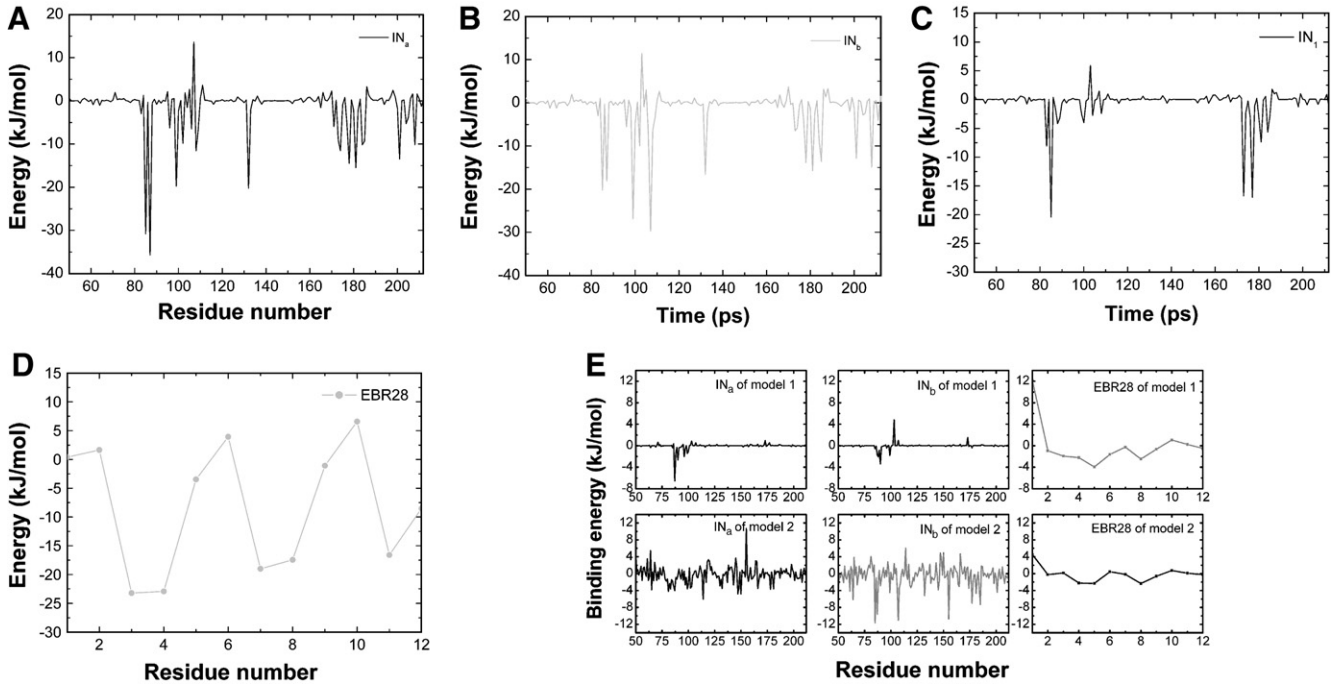

Fig. 10. The interactions between the interfaces of the IN_2, IN_1–EBR28 and IN_2–EBR28 systems. Energy contribution of each residue to the dimerization of IN_2 in the receptor (A) IN_a (colored in black) and the ligand (B) IN_b (colored in gray). Energy contribution of each residue to the association of the receptor (C) IN_1 (colored in black)with the ligand (D) EBR28 peptide (colored in gray). (E) energy contribution of each residue to the dimerization of IN_2–EBR28, and in the two modes, the receptor is represented in black and the ligand is displayed in gray.

to that the hydrophobic side of EBR28 faces IN_b and the hydrophilic one locates near IN_a (see Fig. 4).

In conclusion, the stabilization of IN_2 mainly depends on the interactions between the β3, α1, α5 regions. The formation of IN_1–EBR28 is driven by both the hydrophobic residues (L3, L4, M7 and I8) of EBR28 and the β3, α1, α5 regions of IN_1. In other words, the function of IN_1 is mostly substituted by EBR28. Compared with IN_2, the β3, α1, α5 regions of IN_b are still important for the formation of IN_2–EBR28, however, those of IN_a are ultimately replaced by the dispersed regions of IN_a and the hydrophobic residues of EBR28 in the IN_2–EBR28 system.

3.8. Hypothetical inhibiting mechanism of EBR28

The structures of the docked complexes show that the influence of the association with EBR28 on the catalytic pocket characterized by the conserved DD-35-E motif is very small. This indicates that the previous proposed inhibiting mechanism that EBR28 interacts with the catalytic pocket and inhibit the binding of viral DNA is excluded [12].

By superimposing the structure of IN_1–EBR28 onto that of IN_2, it is found that the position of EBR28 is obviously overlapped by the place of one of the subunit α5 regions in the IN_2 system (Fig. 11) .Thus, the association of IN1 with EBR28 prevents the formation of IN dimmer. In other modeling experiment, the IN_a and IN_b subunits are obtained by manually separating the IN_2 system. Then, a near native IN_a–IN_b complex whose RMSD is 0.152 nm comparing with the initial IN_2 structure can be gained by docking IN_a to IN_b with the RosettaDock package. The near IN_2 structure can not be acquired when IN_b is docked to IN_a–EBR28 formed by the addition of EBR28. As described by Maroun et. al., the association–dissociation reaction equilibrium of IN exist in the AIDS patient. Thus, some types of subunit ensembles simultaneously exist and exhibit dynamic rearrangements [50]. In this work, the binding of IN_1 to EBR28 decreases the concentration of dissociative IN_1 and interferes the formation of the IN_2 dimmer, which inhibits IN from binding with viral DNA in the end. The dimmer structure of IN is necessary for binding viral DNA [10,11].

Through molecular docking, EBR28 inserts into the interspaces of the subunits of IN_2 and forms the IN_2–EBR28

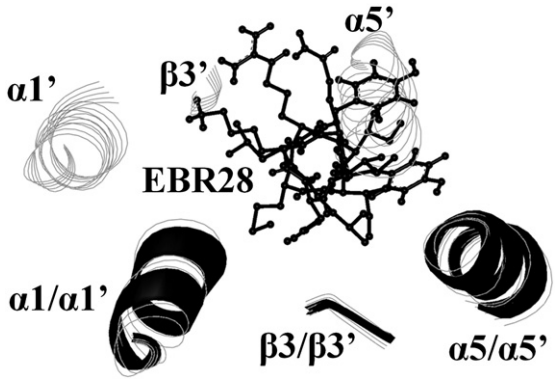

Fig. 11. Superimposing the structure of IN_1–EBR28 onto that of IN_2. The β3, α1, α5 regions of IN_1–EBR28 is represented by black solid-ribbon, and EBR28 is represented by a ball-stick model. The β3, α1, α5 regions structure of IN_2 are shown as a line-ribbon model in gray.

complex, which seems to indicate that the insertion of EBR28 may promote the disassociation of IN_2. In fact, the view is not unreasonable from the following four points: (1) EBR28 has a tendency to translate to outside by analyzing the motive difference of EBR28 in the two docked complexes. The limited MD time is the only reason for the peptide not leaving the binding site in the dimmer–peptide system. (2) The structure and the motion mode of the catalytic region of IN_2 are not influenced by the association with EBR28. (3) The very small separation (0.05 nm) of two subunits resulting from the insertion of EBR28 does not over-influence the viral DNA to bind with the positive charged strip of IN_2. (4) Compared with IN_2, the interactions between the subunits of IN_2_EBR28 do not decrease at all. Thus, it is proposed that the insertion of EBR28 to the interspace of the subunits of IN_2 is not the inhibition mechanism of EBR28.

In conclusion, EBR28 binds to the interface of IN monomer through hydrophobic interactions and prevents the formation of IN dimer, which leads to the partial loss of binding potency for viral DNA with IN.

4. Conclusions

The binding modes between the inhibitor peptide EBR28 with IN_1 and IN_2 were proposed by using molecular docking method. EBR28 interacts with the interfaces (the β3, α1 and α5 regions) of IN_1 and IN_2, which excludes one of the previous views that EBR28 interacts with the catalytic region characterized by the conserved DD-35-E motif.

By comparing the calculated binding free energies between IN_1 and a series of EBR28 mutated peptides with the experimental ones, it is found that the modeling values agree well with the experimental data and the coefficient is 0.88. Thus, the validity of the binding mode between IN_1 and EBR28 is further confirmed. Through using the binding energy decomposition methods to calculate the interactions between interfaces of the IN_1_EBR28, IN_2 and IN_2_EBR28 systems, the bindings of EBR28 to IN_1 and IN_2 are mainly driven by the hydrophobic interactions between the hydrophobic residues of EBR28 and the β3, α1 and α5 regions of IN.

Finally, this work has provided insights into the detailed inhibition mechanism of EBR28. EBR28 binding to the interface of IN_1 which is overlapped by the position corresponding to one of the subunits α5 region of IN_2. Thus, EBR28 serves as affecting the dimerization of IN, which is necessary for HIV-1 IN to bind with viral DNA. Due to the instability of EBR28 in the IN_2_EBR28 system and low influence on the IN_2 structure and its motion mode, the insertion of EBR28 into the interfaces of the IN_2 subunits does not interfere with the association of IN_2 with viral DNA. All the above simulation results are in agreement with the experimental data and provide us with the helpful information for structured-based anti-HIV peptide drug design.

Acknowledgement

This work was supported in part by grants from the National Natural Science Foundation of China (Nos. 30670497 and 30500429) and from Beijing Natural Science Foundation (No. 5072002).

References

[1] F. Barresinoussi, J.C. Chermann, F. Rey, M.T. Nugeyre, S. Chamaret, J. Gruest, C. Dauguet, C. Axlerblin, F. Vezinetbrun, C. Rouzioux, W. Rozenbaum, L. Montagnier, Isolation of a T-lymphotropic retrovirus from a patient at risk for acquired immune-deficiency syndrome (Aids), Science 220 (1983) 868–871.
[2] M. Popovic, M.G. Sarngadharan, E. Read, R.C. Gallo, Detection, isolation, and continuous production of cytopathic retroviruses (Htlv–Iii) from patients with AIDS and pre-AIDS, Science 224 (1984) 497–500.
[3] Y. Pommier, A.A. Johnson, C. Marchand, Integrase inhibitors to treat HIV/AIDS, Nat. Rev. Drug Discov. 4 (2005) 236–248.
[4] D.J. Hazuda, P. Felock, M. Witmer, A. Wolfe, K. Stillmock, J.A. Grobler, A. Espeseth, L. Gabryelski, W. Schleif, C. Blau, M.D. Miller, Inhibitors of strand transfer that prevent integration and inhibit HIV-1 replication in cells, Science 287 (2000) 646–650.
[5] F. Dyda, A.B. Hickman, T.M. Jenkins, A. Engelman, R. Craigie, D.R. Davies, Crystal-Structure of the catalytic domain of Hiv-1 integrase— similarity to other polynucleotidyl transferases, Science 266 (1994) 1981–1986.
[6] Y. Goldgur, R. Craigie, G.H. Cohen, T. Fujiwara, T. Yoshinaga, T. Fujishita, H. Sugimoto, T. Endo, H. Murai, D.R. Davies, Structure of the HIV-1 integrase catalytic domain complexed with an inhibitor: a platform for antiviral drug design, Proc. Natl. Acad. Sci. 96 (1999) 13040–13043.
[7] J.Y. Wang, H. Ling, W. Yang, R. Craigie, Structure of a two-domain fragment of HIV-1 integrase: implications for domain organization in the intact protein, Embo J. 20 (2001) 7333–7343.
[8] S.A. Chow, In vitro assays for activities of retroviral integrase, Methods 12 (1997) 306–317.
[9] P. Gallay, S. Swingler, J.P. Song, F. Bushman, D. Trono, HIV nuclear import is governed by the phosphotyrosine-mediated binding of matrix to the core domain of integrase, Cell 83 (1995) 569–576.
[10] J.C.H. Chen, J. Krucinski, L.J.W. Miercke, J.S. Finer-Moore, A.H. Tang, A.D. Leavitt, R.M. Stroud, Crystal structure of the HIV-1 integrase catalytic core and C-terminal domains: a model for viral DNA binding, Proc. Natl. Acad. Sci. 97 (2000) 8233–8238.
[11] L. De Luca, A. Pedretti, G. Vistoli, M.L. Barreca, L. Villa, P. Monforte, A. Chimirri, Analysis of the full-length integrase-DNA complex by a modified approach for DNA docking, Biochem. Biophys. Res. Commun. 310 (2003) 1083–1088.
[12] V.R. de Soultrait, A. Caumont, V. Parissi, N. Morellet, M. Ventura, C. Lenoir, S. Litvak, M. Fournier, B. Roques, A novel short peptide is a specific inhibitor of the human immunodeficiency virus type 1 integrase, J. Mol. Biol. 318 (2002) 45–58.
[13] V.R. de Soultrait, C. Desjobert, L. Tarrago-Litvak, Peptides as new inhibitors of HIV-1 reverse transcriptase and integrase, Curr. Med. Chem. 10 (2003) 1765–1778.
[14] J.J. Gray, S. Moughon, C. Wang, O. Schueler-Furman, B. Kuhlman, C.A. Rohl, D. Baker, Protein–protein docking with simultaneous optimization of rigid-body displacement and side-chain conformations, J. Mol. Biol. 331 (2003) 281–299.
[15] B. Kuhlman, D. Baker, Native protein sequences are close to optimal for their structures, Proc. Natl. Acad. Sci. 97 (2000) 13460.
[16] M.D. Daily, D. Masica, A. Sivasubramanian, S. Somarouthu, J.J. Gray, CAPRI rounds 3–5 reveal promising successes and future challenges for RosettaDock, Proteins 60 (2005) 181–186.
[17] J.J. Gray, S.E. Moughon, T. Kortemme, O. Schueler-Furman, K.M.S. Misura, A.V. Morozov, D. Baker, Protein–protein docking predictions for the CAPRI experiment, Proteins-Struct. Funct. Genet. 52 (2003) 118–122.
[18] J. Janin, K. Henrick, J. Moult, L. Ten Eyck, M.J.E. Sternberg, S. Vajda, I. Vasker, S.J. Wodak, CAPRI: A Critical Assessment of PRedicted Interactions, Protein-Struct. Funct. Genet. 52 (2003) 2–9.
[19] D. Petrey, Z.X. Xiang, C.L. Tang, L. Xie, M. Gimpelev, T. Mitros, C.S. Soto, S. Goldsmith-Fischman, A. Kernytsky, A. Schlessinger, I.Y.Y. Koh, E. Alexov, B. Honig, Using multiple structure alignments, fast model building,

and energetic analysis in fold recognition and homology modeling, Protein-Struct. Funct. Genet. 53 (2003) 430–435.
[20] W. Kabsch, C. Sander, Dictionary of protein secondary structure— pattern-recognition of hydrogen-bonded and geometrical features, Biopolymers 22 (1983) 2577–2637.
[21] V. Munoz, L. Serrano, Development of the multiple sequence approximation within the AGADIR model of alpha-helix formation: comparison with Zimm–Bragg and Lifson–Roig formalisms, Biopolymers 41 (1997) 495–509.
[22] M.L. Cai, R.L. Zheng, M. Caffrey, R. Craigie, G.M. Clore, A.M. Gronenborn, Solution structure of the N-terminal zinc binding domain of HIV-1 integrase, Nat. Struct. Biol. 4 (1997) 567–577.
[23] Y. Goldgur, F. Dyda, A.B. Hickman, T.M. Jenkins, R. Craigie, D.R. Davies, Three new structures of the core domain of HIV-1 integrase: an active site that binds magnesium, Proc. Natl. Acad. Sci. 95 (1998) 9150–9154.
[24] G. Bujacz, M. Jaskolski, J. Alexandratos, A. Wlodawer, G. Merkel, R.A. Katz, A.M. Skalka, The catalytic domain of avian sarcoma virus integrase: Conformation of the active-site residues in the presence of divalent cations, Structure 4 (1996) 89–96.
[25] J.M. Wang, P. Cieplak, P.A. Kollman, How well does a restrained electrostatic potential (RESP) model perform in calculating conformational energies of organic and biological molecules? J. Comput. Chem. 21 (2000) 1049–1074.
[26] J.M. Wang, R.M. Wolf, J.W. Caldwell, P.A. Kollman, D.A. Case, Development and testing of a general amber force field, J. Comput. Chem. 25 (2004) 1157–1174.
[27] W.D. Cornell, P. Cieplak, C.I. Bayly, I.R. Gould, K.M. Merz, D.M. Ferguson, D.C. Spellmeyer, T. Fox, J.W. Caldwell, P.A. Kollman, A second generation force field for the simulation of proteins, nucleic acids, and organic molecules, J. Am. Chem. Soc. 117 (1995) 5179–5197.
[28] S.W. Homans, A molecular mechanical force-field for the conformational analysis of oligosaccharides— comparison of theoretical and crystal-structures of Man-Alpha-1-3man-Beta-1-4glcnac, Biochemistry 29 (1990) 9110–9118.
[29] S.J. Weiner, P.A. Kollman, D.A. Case, U.C. Singh, C. Ghio, G. Alagona, S. Profeta, P. Weiner, A new force-field for molecular mechanical simulation of nucleic-acids and proteins, J. Am. Chem. Soc. 106 (1984) 765–784.
[30] S.J. Weiner, P.A. Kollman, D.T. Nguyen, D.A. Case, An all atom force-field for simulations of proteins and nucleic-acids, J. Comput. Chem. 7 (1986) 230–252.
[31] W.L. Jorgensen, J. Chandrasekhar, J.D. Madura, R.W. Impey, M.L. Klein, Comparison of simple potential functions for simulating liquid water, J. Chem. Phys. 79 (1983) 926–935.
[32] J.P. Ryckaert, G. Ciccotti, H.J.C. Berendsen, Numerical-integration of Cartesian equations of motion of a system with constraints— molecular-dynamics of n-alkanes, J. Comput. Phys. 23 (1977) 327–341.
[33] A. Amadei, A.B.M. Linssen, H.J.C. Berendsen, Essential dynamics of proteins, Protein-Struc. Funct. Genet. 17 (1993) 412–425.
[34] A. Amadei, A.B.M. Linssen, B.L. De Groot, D.M.F. Van Aalten, H.J.C. Berendsen, An efficient method for sampling the essential subspace of proteins, J. Biomol. Struct. Dyn. 13 (1996) 615–626.
[35] B.L. De Groot, A. Amadei, R.M. Scheek, N.A.J. Van Nuland, H.J.C. Berendsen, An extended sampling of the configurational space of HPr from *E. coli*, Protein-Struct. Funct. Genet. 26 (1996) 314–322.
[36] R. Abseher, M. Nilges, Efficient sampling in collective coordinate space, Protein-Struct. Funct. Genet. 39 (2000) 82–88.
[37] P.A. Kollman, I. Massova, C. Reyes, B. Kuhn, S.H. Huo, L. Chong, M. Lee, T. Lee, Y. Duan, W. Wang, O. Donini, P. Cieplak, J. Srinivasan, D.A. Case, T.E. Cheatham, Calculating structures and free energies of complex molecules: combining molecular mechanics and continuum models, Acc. Chem. Res. 33 (2000) 889–897.
[38] W. Wang, O. Donini, C.M. Reyes, P.A. Kollman, Biomolecular simulations: Recent developments in force fields, simulations of enzyme catalysis, protein–ligand, protein–protein, and protein–nucleic acid noncovalent interactions, Annu. Rev. Biophys. Biomol. Struct. 30 (2001) 211–243.
[39] D. Bashford, D.A. Case, Generalized born models of macromolecular solvation effects, Annu. Rev. Phys. Chem. 51 (2000) 129–152.
[40] T. Simonson, Macromolecular electrostatics: continuum models and their growing pains, Curr. Opin. Struck. Biol. 11 (2001) 243–252.
[41] V. Tsui, D.A. Case, Theory and applications of the generalized Born solvation model in macromolecular simulations, Biopolymers 56 (2000) 275–291.
[42] D. Sitkoff, K.A. Sharp, B. Honig, Accurate calculation of hydration free-energies using macroscopic solvent models, J. Phys. Chem. 98 (1994) 1978–1988.
[43] J. Kottalam, D.A. Case, Langevin modes of macromolecules— applications to Crambin and DNA hexamers, Biopolymers 29 (1990) 1409–1421.
[44] W.C. Still, A. Tempczyk, R.C. Hawley, T. Hendrickson, Semianalytical treatment of solvation for molecular mechanics and dynamics, J. Am. Chem. Soc. 112 (1990) 6127–6129.
[45] J. Weiser, P.S. Shenkin, W.C. Still, Approximate atomic surfaces from linear combinations of pairwise overlaps (LCPO), J. Comput. Chem. 20 (1999) 217–230.
[46] C.X. Wang, Y.Y. Shi, F. Zhou, L. Wang, Thermodynamic integration calculations of binding free-energy difference for Gly-169 mutation in subtilisin BPN, Protein-Struct. Funct. Genet. 15 (1993) 5–9.
[47] A.J. Doig, M.J.E. Sternberg, Side-chain conformational entropy in protein-folding, Protein Sci. 4 (1995) 2247–2251.
[48] T.J. Hou, S.L. Guo, X.J. Xu, Predictions of binding of a diverse set of ligands to gelatinase-A by a combination of molecular dynamics and continuum solvent models, J. Phys. Chem., B 106 (2002) 5527–5535.
[49] B. Kuhn, P.A. Kollman, Binding of a diverse set of ligands to avidin and streptavidin: an accurate quantitative prediction of their relative affinities by a combination of molecular mechanics and continuum solvent models, J. Med. Chem. 43 (2000) 3786–3791.
[50] R.G. Maroun, S. Gayet, M.S. Benleulmi, H. Porumb, L. Zargarian, H. Merad, H. Leh, J.F. Mouscadet, F.R. Troalen, S. Fermandjian, Peptide inhibitors of HIV-1 integrase dissociate the enzyme oligomers, Biochemistry 40 (2001) 13840–13848.